FACULTAD DE CIENCIAS DEL MAR

THE BOUNDARY CURRENTS AT 24ºS: THE BRAZIL AND THE BENGUELA CURRENTS, AND THE NADW IN THE DEEP WESTERN AND EASTERN BOUNDARIES

Daniel Santana Toscano

Curso 2018/2019

Tutor: Dr. Alonso Hernández Guerra

Cotutora: María Casanova Masjoan

IOCAG Instituto de Oceanografía y Cambio Global

The Boundary Currents at 24ºS: the Brazil and the Benguela Currents, and the NADW in the Deep Western and Eastern Boundaries

by

Daniel Santana Toscano

Submitted in fulfilment of the requirements for:

GRADO EN CIENCIAS DEL MAR

at

UNIVERSIDAD DE LAS PALMAS DE GRAN CANARIA

Signature of Author……Daniel Santana Toscano…….

FACULTAD DE CIENCIAS DEL MAR

UNIVERSIDAD DE LAS PALMAS DE GRAN CANARIA

Signature of Tutor……Alonso Hernández Guerra……..

INSTITUTO DE OCEANOGRAFÍA Y CAMBIO GLOBAL

DEPARTAMENTO DE FÍSICA

FACULTAD DE CIENCIAS DEL MAR

UNIVERSIDAD DE LAS PALMAS DE GRAN CANARIA

Signature of co-Tutor……María Casanova Masjoan……..

INSTITUTO DE OCEANOGRAFÍA Y CAMBIO GLOBAL

DEPARTAMENTO DE FÍSICA

FACULTAD DE CIENCIAS DEL MAR

UNIVERSIDAD DE LAS PALMAS DE GRAN CANARIA

Las Palmas De Gran Canaria, May 2019

Table of Contents

Abstract

The Brazil and Benguela Currents and the North Atlantic Deep Water flow in the Atlantic Ocean at 24°S in 2009 are studied by the implementation of an inverse model with GO-SHIP hydrographic data. Additionally, the net meridional transports of mass, heat and freshwater are calculated. The Brazil Current flows over the westernmost stations with a mass transport of -3.3±1.0 Sv to the south. Meanwhile, the Benguela Current System flows northward with a transport of 13.2±3.3 Sv. The Deep Western Boundary Current drives the North Atlantic Deep Water from the north to the south of the Atlantic Ocean, where it splits into two branches. One of them flows through the western boundary and the other flows from the middle of the South Atlantic Ocean to its eastern boundary, the net transport of the NADW is -25.5±1.3 Sv. The heat transport shows a northward flux of 1.0±0.1 PW, higher than previous studies. The freshwater budget showcases a -0.8±0.2 Sv transport from the ocean to the atmosphere (evaporation), matching the results of previous studies.

1. Introduction

The subtropical gyres are characterized by an equatorward Sverdrup transport (Sverdrup, 1947) and a returning flow portrayed by the Western Boundary Current (WBC) (Stommel, 1948; Munk, 1950). In particular, the South Atlantic's subtropical gyre is a wind-driven structure limited by two currents: the Brazil Current (BC) and the Benguela Current System (BCS), which are the western and eastern (EBC) boundary currents, respectively. The equatorward flow is partially driven by the leakage of the Agulhas Current (AC) in Cape Agulhas (Talley et al., 2011). Additionally, approximately six out of nine Agulhas rings that are released per year in the Agulhas Retroflection reach the eastern coast of America with a rotating transport of 20-30 Sv (1 Sv = 10^6 $m^3/s \approx 10^9$ Kg/s) (Casanova-Masjoan et al., 2017). Schmid & Majumder (2018) estimated the BC and the BCS with transports of -4.4±1.4 Sv (negative southwards) over 24ºS and 9.6±2.8 Sv over 25ºS, respectively.

The water masses found in the gyre are the South Atlantic Central Water (SACW), Antarctic Intermediate Water (AAIW), Upper Circumpolar Deep Water (UCDW), North Atlantic Deep Water (NADW) and Antarctic Bottom Water (AABW) (Appendix). The main water mass studied in this work is the NADW, which is originated in the subpolar North Atlantic Ocean and is composed by Labrador Sea Water (LSW) (Rhein et al., 2002), Denmark Strait Overflow Water (DSOW), Iceland Scotland Overflow Water (ISOW) (García-Ibáñez et al., 2015) and Mediterranean Water (MW) (Bashmachnikov et al., 2015; Zenk et al., 1990). The fluctuation of these sources creates a variability wherein

the NADW that should be described. The NADW has two branches at 24ºS, both of them come from an earlier division of LSW (Ferreira & Kerr, 2017).

The heat budget of the ocean is a key parameter for understanding the Earth's climate system, as it is known that the global ocean transports from one-third to one-half of the total excess heat from the tropics to the poles (Talley, 2003). Both heat and freshwater budgets are the most important features of the overturning circulation: the difference of this properties between water masses forces them to sink or rise in the water column, creating the pattern of the thermohaline circulation (THC). For 24ºS, Bryden et al. (2011) estimated that the heat and freshwater meridional fluxes are 0.7±0.1 PW (1 PW = 10^{15} W) and -0.8±0.2 Sv, respectively. Thus, in this work we expect to find equatorward heat and freshwater fluxes.

The aim of the work is to investigate with an inverse method (Wunsch, 1996) the contribution of the water masses and the boundary currents to the meridional transports of mass, heat and freshwater and the distribution of the NADW at the A095 hydrographic section (24ºS) surveyed between March and April of 2009.

The study is organized as follows: section 2 presents the hydrographic data sets, the vertical structure of the water properties and the water masses that are found in the A095 transect; section 3 introduces the mass-unbalanced meridional transports as preliminary results and explains how the inverse model is implemented; section 4 is focused on the mass-balanced meridional transports and section 5 will discuss the final results and highlight some conclusions.

2. Data, Vertical Sections and Water Masses

Conductivity-Temperature-Depth (CTD) profiles and bottle samples of oxygen and silicates were collected from the Global Ocean Ship-based Hydrographic Investigations Program (GO-SHIP) (Talley et al., 2016). They were extracted from stations 23 to 118 of 2009 South Atlantic's A095 section (Fig. 1), with a mean distance between stations of 60 km. We did not include the first 22 stations because they were placed to measure the BC in higher latitudes. Moreover, station 36 has not been included because its geographical coordinates do not correspond to the real position where the cruise was carried out and data of station 48 did not appear in the data set.

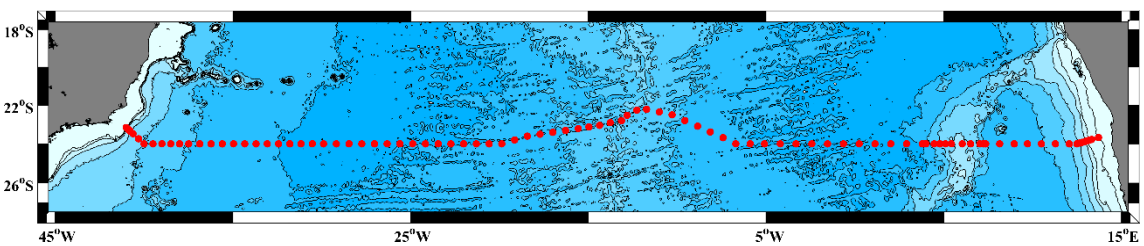

Fig. 1. South Atlantic's A095 Transect 24°S - 23-118 Stations Locations

The vertical sections of potential temperature, salinity, oxygen, silicates and neutral density are shown in Figures 2-6. The vertical sections together with the θ/S diagram (Fig. 7) will allow us to know the vertical and spatial distribution of the different water masses existing in the region.

The SACW is a subducted water mass formed in the South Atlantic's subtropical gyre. The origin of the subducted waters is the leakage of the AC into the Atlantic Ocean and the confluence of the BC and the Malvinas Current (MC) (Sprintall & Tomczak, 1993). The SACW extends from the surface to the density interface of γ^n=27.3 kg/m^3 (~750 metres depth). Also, it defines the thermocline layer with high salinity (>34.5 psu), high oxygen (>190 µM/kg) and very low silicates (<20 µM/kg) values.

The major source of AAIW flowing into the Atlantic Ocean is the convective overturning in the south-eastern Pacific (Suga & Talley, 1995). This water mass occupies the range between γ^n=27.3 kg/m^3 and γ^n=27.72 kg/m^3 (750-1300 m) and it is characterized by low salinity (<34.5 psu), low oxygen (<190 µM/kg) and moderate silicates values (<40 µM/kg).

Further deep, the UCDW is the upper branch of the Circumpolar Deep Water (CDW) that has been divided into two branches by the NADW (Reid, 1989). The UCDW extends from γ^n=27.72 kg/m^3 to γ^n=27.903 kg/m^3 (1300-1750 m) and is characterized by moderate salinity values (34.7-34.9 psu), a higher oxygen concentration than the AAIW (190-220 µM/kg) and a local maximum of silicates (>40 µM/kg).

The NADW is an entrance of north Atlantic water transported to the south by the Deep Western Boundary Current (DWBC) (Stommel, 1948) within the γ^n=27.903 kg/m^3 and γ^n=28.11 kg/m^3 neutral density interfaces (1750-3500 m) (Tsuchiya, Talley, & McCartney, 1994). This water mass is easily recognizable in the western basin of Figs. 3-5 because of its high salinity (>34.9 psu), high oxygen (>240 µM/kg) and low silicate values (<40 µM/kg). The water mass is also recognized in the eastern basin of Fig. 5 because of its low silicate values (<40 µM/kg) (Larque et al., 1979).

The sources of the AABW are CDW, high density and salinity shelf waters and melted ice waters (Ferreira & Kerr, 2017). It extends from our selected level of no-motion γ^n=28.11 kg/m^3 (Ganachaud, 1999; McDonagh & King, 2005) at 3500 metres to the bottom of the ocean. It is a less saline (<34.9 psu) and less oxygenated (<240 µM/kg) water than the NADW (Reid, 1989). The silicates, on the contrary, are significantly higher as they reach their maximum value (>80µM/kg).

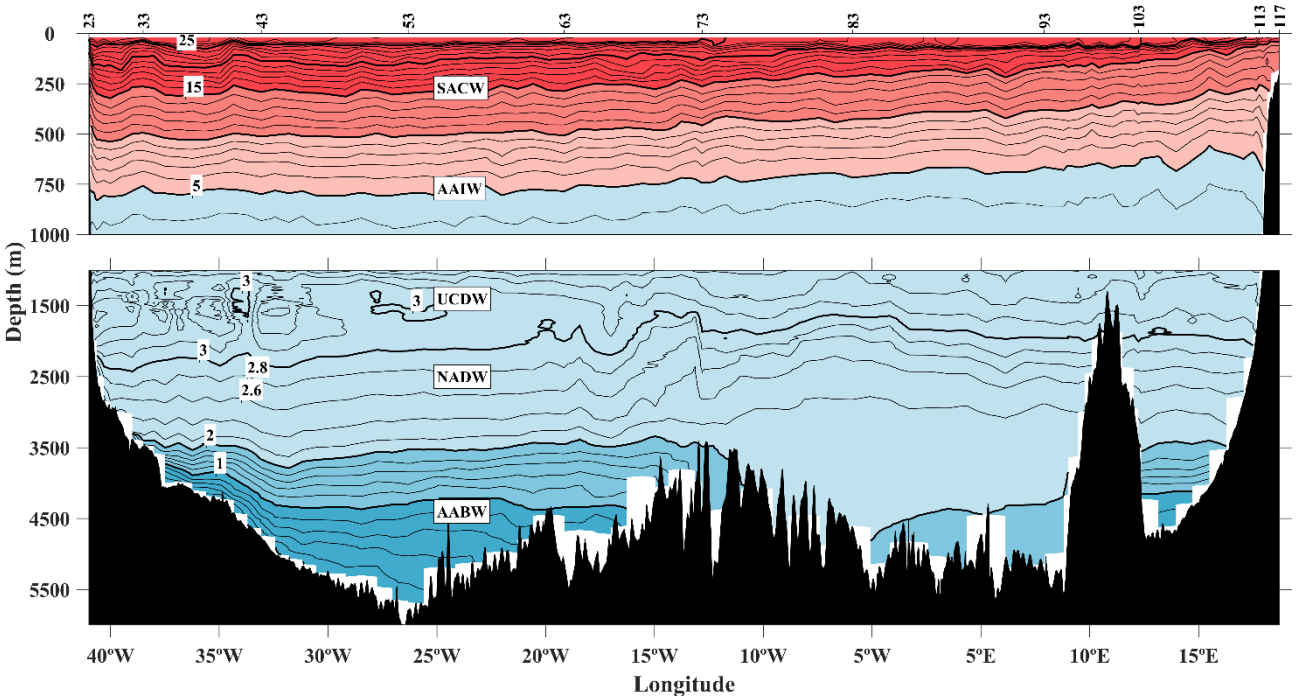

Fig. 2. Vertical section of potential temperature (ºC) for the Atlantic Ocean at 24ºS in 2009

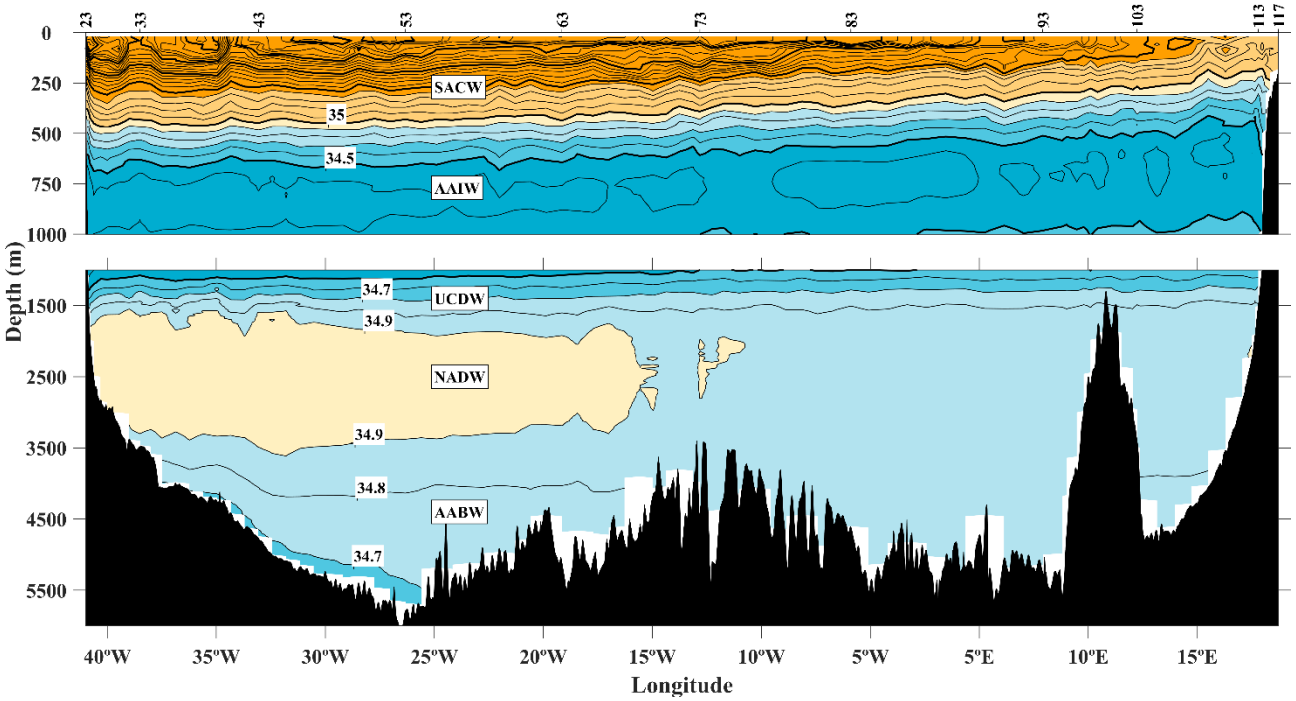

Fig. 3. Vertical section of salinity (psu) for the Atlantic Ocean at 24ºS in 2009

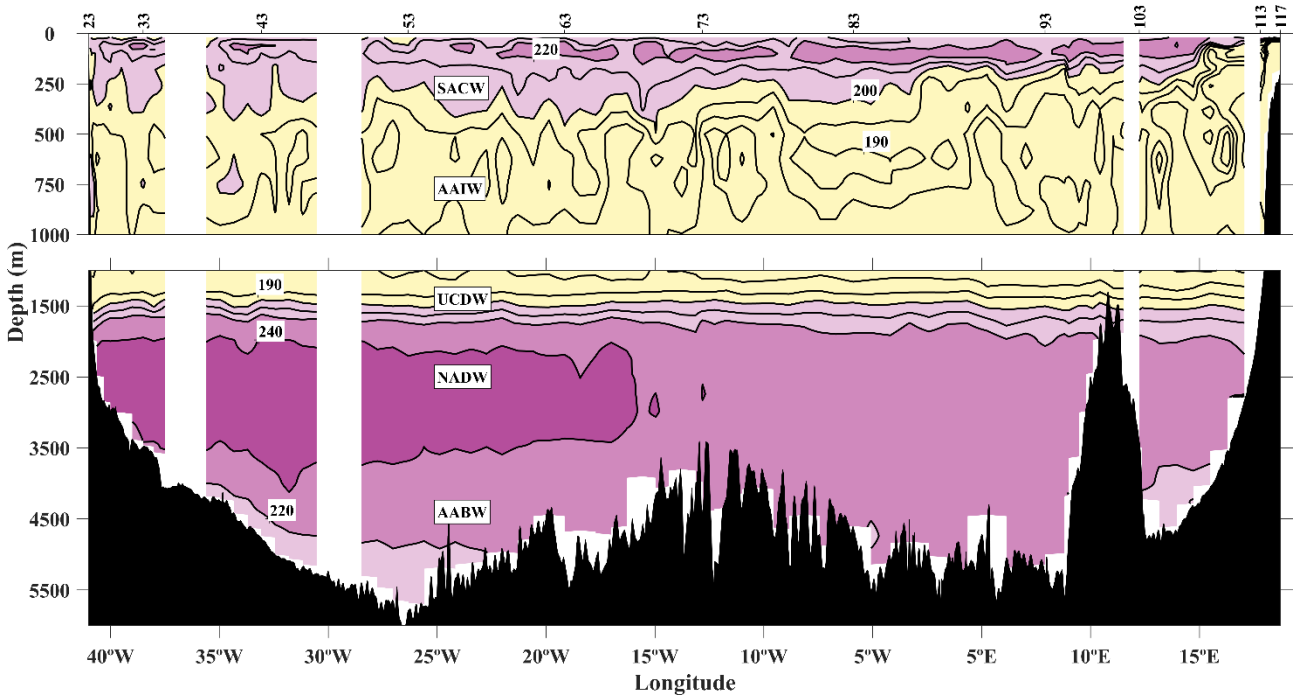

Fig. 4. Vertical section of oxygen (µM/kg) for the Atlantic Ocean at 24ºS in 2009

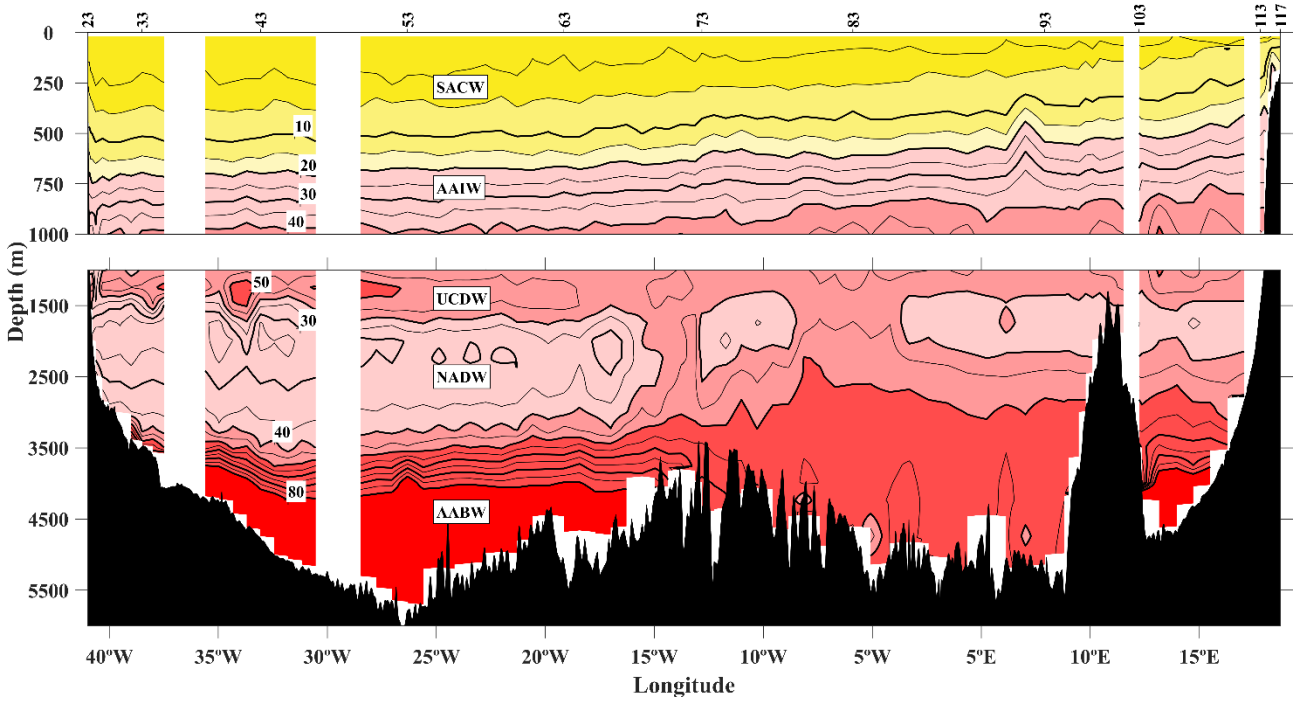

Fig. 5. Vertical section of silicates (µM/kg) for the Atlantic Ocean at 24ºS in 2009

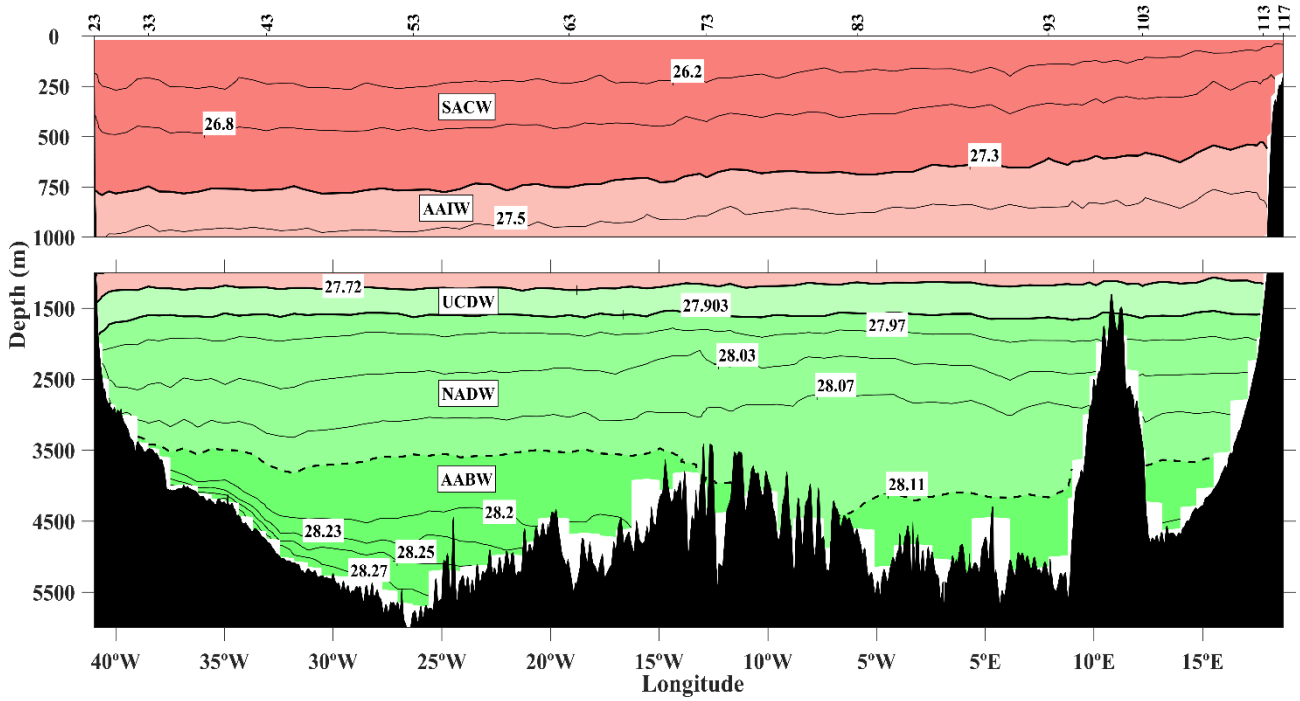

Fig. 6. Vertical section of gamma (kg/m^3) for the Atlantic Ocean at 24ºS in 2009

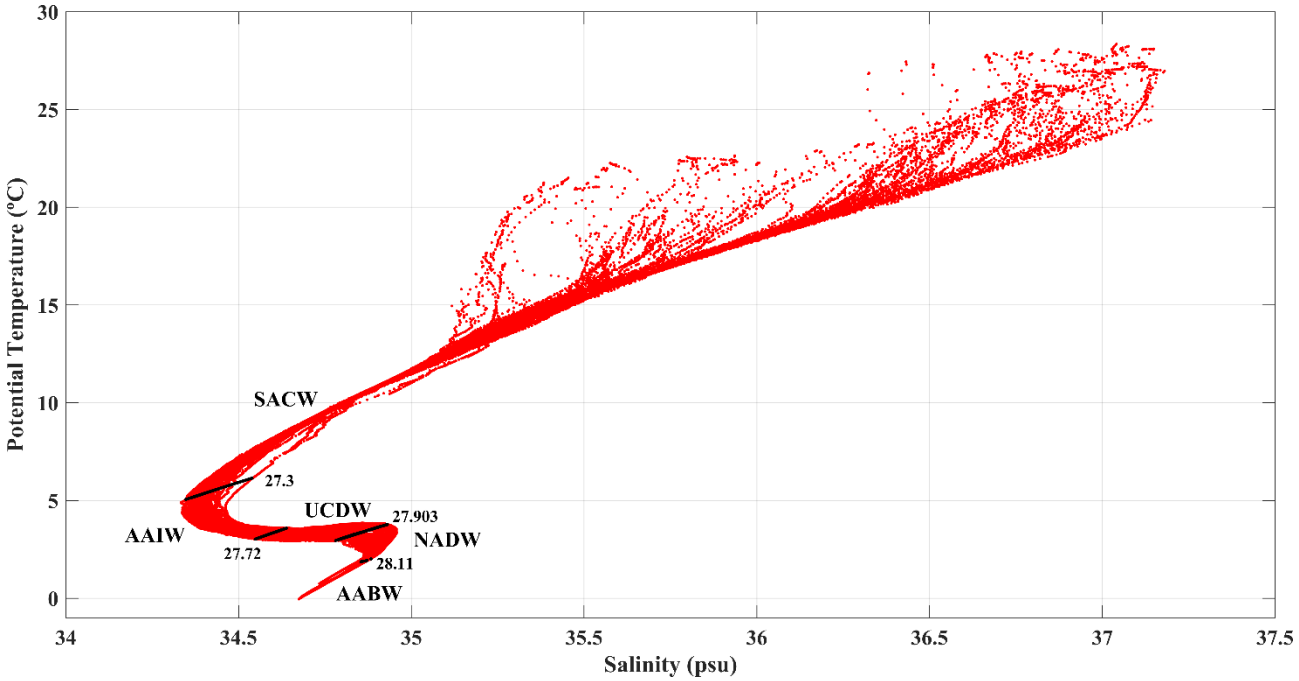

Fig. 7. Potential Temperature/Salinity Diagram for the Atlantic Ocean at 24ºS in 2009. The blacksolid lines are the water masses divisions by neutral density interfaces (kg/m^3).

3. Methodology and Initial Transports

The vertical distributions of potential temperature, salinity, oxygen, silicates and neutral density (Figs. 2-6) and the θ/S diagram (Fig. 7) were used to know the different water masses and also to calculate the relative geostrophic velocities and the initial transports following the method of Hernández-Guerra & Talley (2016). We have followed the studies of Ganachaud (1999) and McDonagh & King (2005) that suggest 4 water masses, 16 neutral surface layers and a level of no-motion (dashed line in Fig 6) between the NADW and the AABW to be used in the thermal-wind equation (Table 1). For station pairs that are shallower than this depth, the level of no-motion is the shallowest depth between the two stations.

Table 1
Neutral Surface Layers γ^n (kg/m^3) and level of no-motion (in bold) in the South Atlantic. Ganachaud (1999) and McDonagh & King (2005)

Layer	Upper Interface Surface	Water Mass
1	-	SACW
2	$\gamma^n = 26.2$	
3	$\gamma^n = 26.8$	
4	$\gamma^n = 27.3$	AAIW
5	$\gamma^n = 27.5$	
6	$\gamma^n = 27.72$	UCDW
7	$\gamma^n = 27.903$	NADW
8	$\gamma^n = 27.97$	
9	$\gamma^n = 28.03$	
10	$\gamma^n = 28.07$	
11	**$\gamma^n = 28.11$**	AABW
12	$\gamma^n = 28.20$	
13	$\gamma^n = 28.23$	
14	$\gamma^n = 28.25$	
15	$\gamma^n = 28.27$	
16	$\gamma^n = 28.296$	

In addition to the initial transport, the mean Ekman transport (Kanamitsu et al., 2002) calculated from NCEP–DOE Atmospheric Model Intercomparison Project reanalysis (AMIP-II) has been included in the first layer of the transect with a value of -1.5±0.1 Sv. Two different ways of estimating the Ekman transport to the first layer have been used:

Ganachaud (2003) uses the long-term mean transport of the year and Hernández-Guerra & Talley (2016) use the mean Ekman transport of the time of the cruise.

The initial mass transport for the A095 transect in 2009 (Fig. 8) is 11 Sv at the surface (positive northward) and it decreases almost lineally until the γ^n=27.97 kg/m^3 layer, where it slightly changes to a southward flow (~ 0.4 Sv) until the next layer γ^n=28.03 kg/m^3. The flow continues to the north until the bottom.

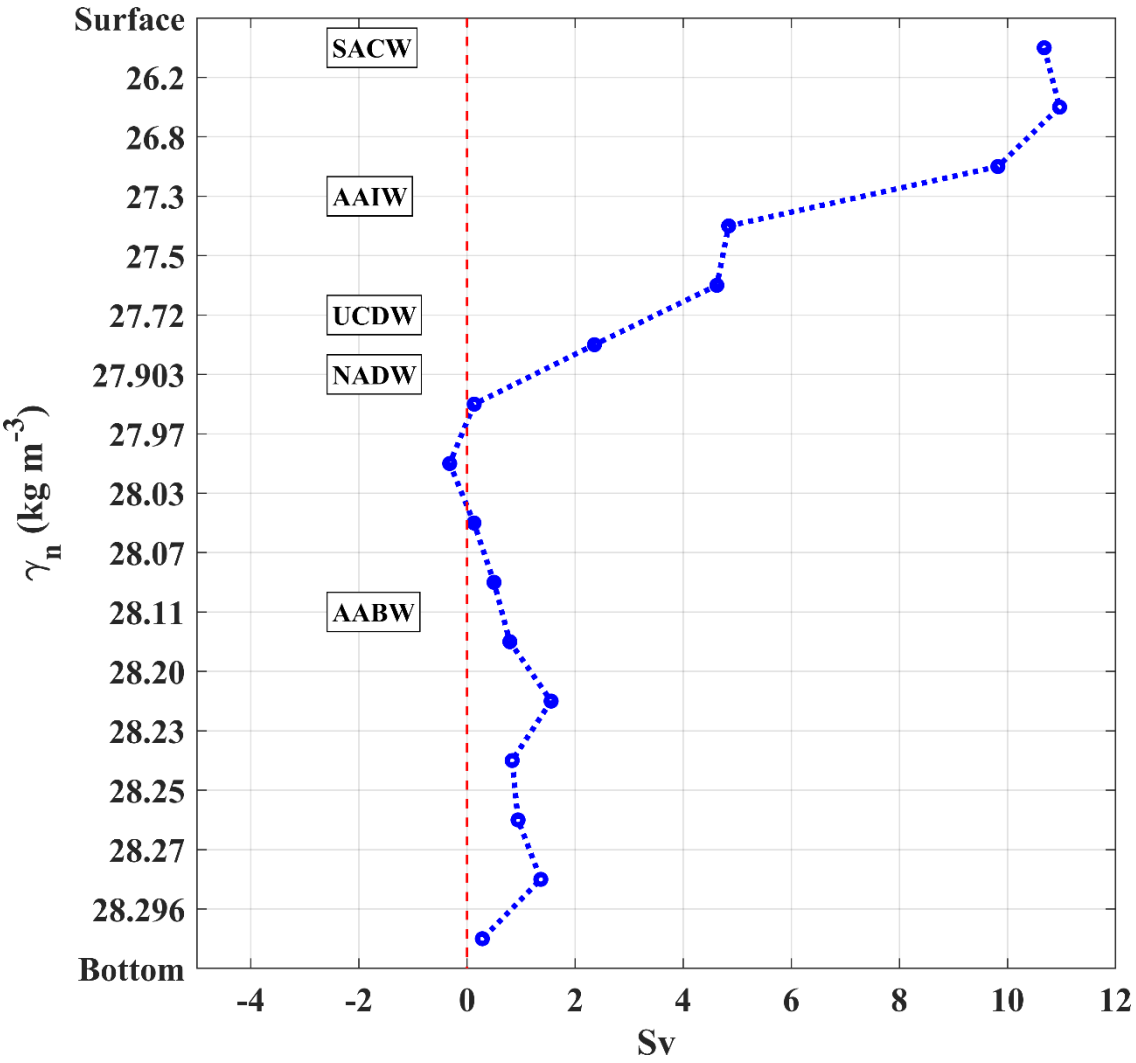

Fig. 8. Initial Meridional Mass Transport (Sv) in the Atlantic Ocean at 24ºS in 2009

Another way of analysing the meridional transport is to observe its horizontal distribution between neutral density layers, for which we integrate eastwards and layer by layer the transport values. The starting station to integrate is the westernmost station. Fig. 9 shows the accumulated mass transport following this procedure: where we show three different accumulated flows: the surface (red), deep (dark blue), bottom (light blue) and total (black) transports.

The flowing pattern of the superficial waters (SACW and AAIW) is clearly northward (positive northward and negative southward), so it qualitatively agrees with previous studies (Sprintall & Tomczak, 1993; Suga & Talley, 1995).

The deep waters (UCDP and NADW) show a non-clear structure along the transect. It is supposed to be a strong southward flux in the west because of the DWBC and another intense flux between -10ºW – 0ºE due to a split of the DWBC that occurs in lower latitudes (Ferreira & Kerr, 2017).

The bottom waters (AABW) don't flow over the westernmost part of the transect because the bottom of the ocean is shallower in this zone (Fig. 6). Nonetheless, there is a weak northward flux over the remaining basin that also agrees with previous works (Ferreira & Kerr, 2017).

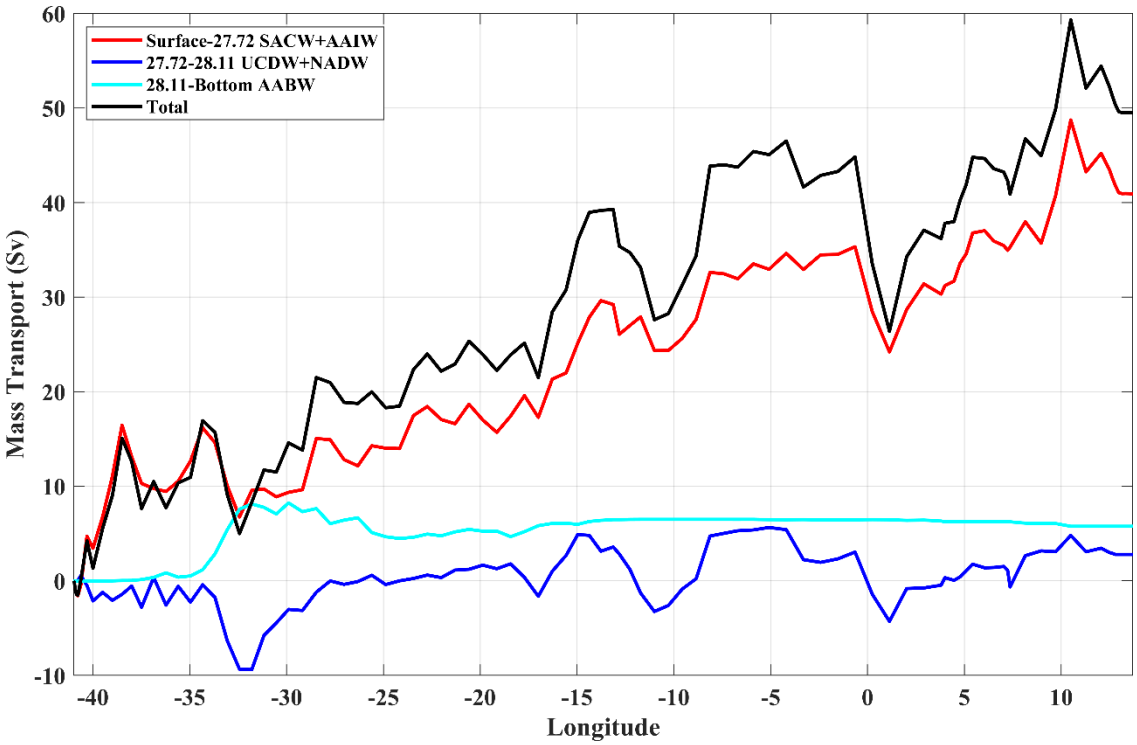

Fig. 9. Integrated mass transport (Sv) for the Atlantic Ocean at 24°S in 2009. The integration begins in the east at the coast of South America. Positive accumulated mass transport is northward. The legend shows the neutral surface layers γ^n (kg/m^3) where the waters masses spread.

3.1 Inverse Box Model

The inverse box models are generally used in oceanography for estimating the geostrophic velocities at the reference layer, taking into account several constraints applicable to the region and time of study with their respective uncertainties (Table 2). The basics of inverse methods applied to geophysics and oceanography will not be thoroughly discussed here, but if the reader is interested in the matter, a study of the

pioneering work of Backus & Gilbert (1967), its later review by Parker (1977) and its implementation in oceanography by Wunsch (1996) is strongly recommended. As shown in Hernández-Guerra & Talley (2016), the inverse problem can be stated as follows:

$$\mathbf{Ab} + \mathbf{n} = \mathbf{Y} \qquad \text{(Eq. 1)}$$

where **A** is a MxN matrix (M is the number of transport constraints and N is the number of unknowns) with information about the mass enclosed between layers and station pairs, **b** is a column vector of length N containing the unknown geostrophic reference velocities, plus the adjustment to the Ekman transport, **n** is a column vector of length M of the noise of each constraint, and **Y** is a column vector of length M with elements equal to the sum of the initial transports (based on geostrophic velocities), the estimated transports (that are applied as constraints) and the Ekman transports.

Table 2
Constraints applied to the Inverse Model

Constraint	Value (Sv)	Reference
Bering Imbalance in Total Mass Conservation	-0.8±0.6	Coachman & Aagaard (1988)
Northward AABW over the Brazil Basin	6.9±1.8	Hogg et al. (1999)
No Abyssal Flux over the Northern Walvis Ridge (WR)	0±1.2	Warren & Speer (1991)
BC	-4.4±1.4	Schmid & Majumder (2018)

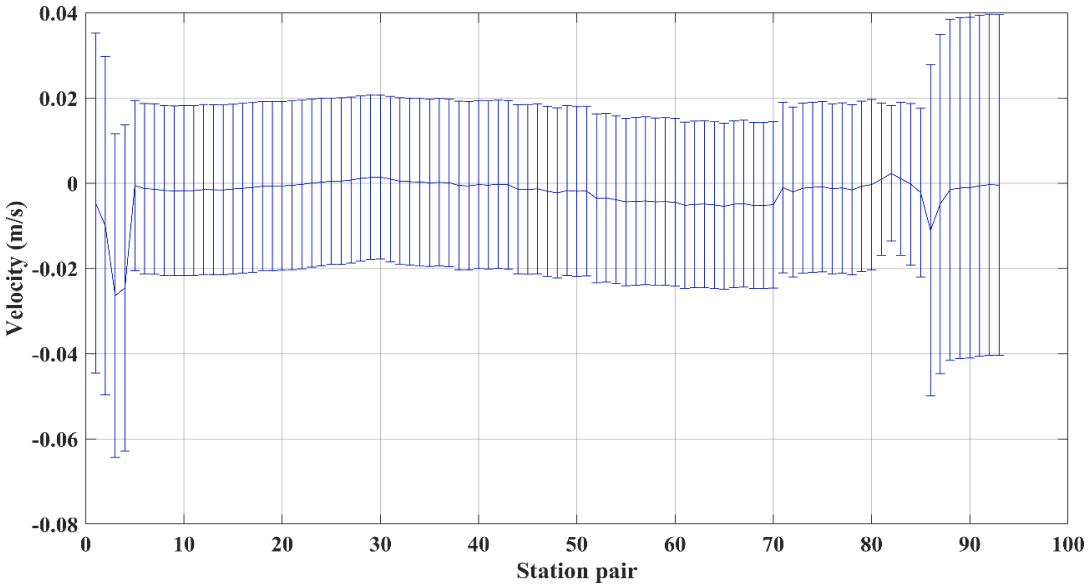

Fig. 10. Velocity at the Reference Layer (with error bars) per station pair from (W-E) in the Atlantic Ocean at 24ºS in 2009

One of the most common methods of solving the inverse model is the Gauss-Markov method (Wunsch, 1996), which needs an a priori set of velocity variances. Here, we used the same approach as Hernández-Guerra & Talley (2016) for this variances: $(0.02\ m/s)^2$ in general and $(0.04\ m/s)^2$ for regions with a very strong shear (areas shallower than 2000 m depth in this work).

In Fig. 10, we can see that the adjusted reference velocities at the assumed level of no-motion are not significantly different from zero in the whole transect, with variances very close to the a priori ones.

4. Adjusted Meridional Transports

The initial (unbalanced) net transport at 24ºS in the South Atlantic is 11 Sv (positive northward). After applying the inverse model, the net flux is consistent with the Bering Strait transport constraint (Table 2) of -0.8±0.3 Sv and, therefore, the model is working correctly.

The structure of the zonally integrated meridional mass transport is in Fig. 11, where we differentiate three fluxes depending on their depth: the upper northward (positive) flow conformed by the SACW and the AAIW, the stronger and deeper southward (negative) flow shaped by the UCDW and the NADW, and the weak bottom flow portrayed by the AABW. Each layer has a mean transport value and an error associated to it (horizontal lines), the higher errors correspond to the deep layers (mainly NADW) and they can be caused either by the correction of the initial mass flux, that was firstly above zero at this level (Fig. 8) and/or by the intrinsic higher variability of the NADW along the whole transect: stronger in the western basin and much weaker in the eastern basin (Ferreira & Kerr, 2017; Stommel et al., 1958; Warren & Speer, 1991).

As it was specified before, the meridional transport can be analysed by observing the horizontal distribution between neutral density layers (horizontal-eastward layer by layer integrated transport) (Fig. 12). Fig. 12 is the analogous of Fig. 9 and the same colours have been used between the two figures in order to facilitate the comparison: surface flow is red, deep flow is dark blue, bottom flow is light blue and total flow is black. The pattern of the flow is almost conserved when the flow is mass-balanced, but it differs greatly in a quantitative view (Figs. 8-11): the balanced result shows a more intense and wider NADW flowing southwards (Stommel, Arons, & Faller, 1958; Warren & Speer, 1991).

The accumulated mass transport for the upper ocean (red line) behaves accordingly to the subtropical gyre: in the western limit the WBC (BC) is presented as a transport of -3.3 Sv to the south (partially covered with AAIW flowing northward) and a recirculation in the remaining basin contrary to the direction of the boundary current. At the eastern

end of the figure (~10ºE), the BCS is depicted by the peak of 13.2 Sv in the upper waters and deep waters.

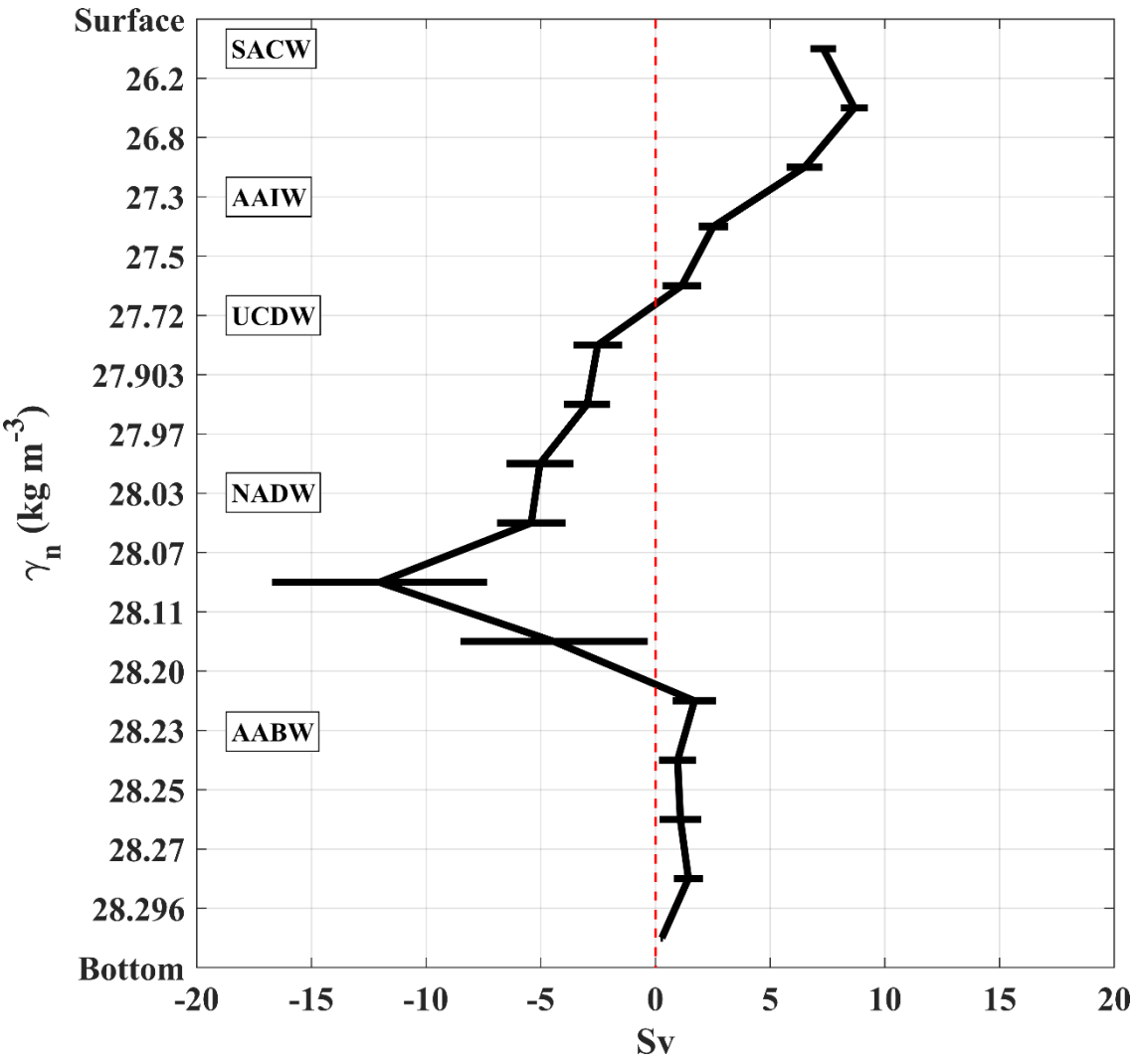

Fig. 11. Mass Transport (mass-balanced) with error bars for each layer in the Atlantic Ocean at 24ºS in 2009

The principal flow of deep waters (blue line) through this transect occurs from 14ºW to 2ºE, where there is a -20.1±0.7 Sv mass transport to the south. What we intrinsically see is one of the branches of the DWBC flowing strongly to the south. The other branch of the NADW is located at 34-32ºW and it is much weaker than the first one (-5.4±1.1 Sv). We do not have other major transports flowing through this zone because we are in the middle latitudes of the subtropical gyre (Talley et al., 2011).

In the bottom layers of the meridional transport, the AABW is the only water mass flowing over the whole section. The flow matches the expected pattern: no transport through the western end of the section because of the shallower depths and a steady flow over the section until its decay to almost 0 Sv in the northern Walvis Ridge (WR) at 5ºE (Table 2) (Warren & Speer, 1991).

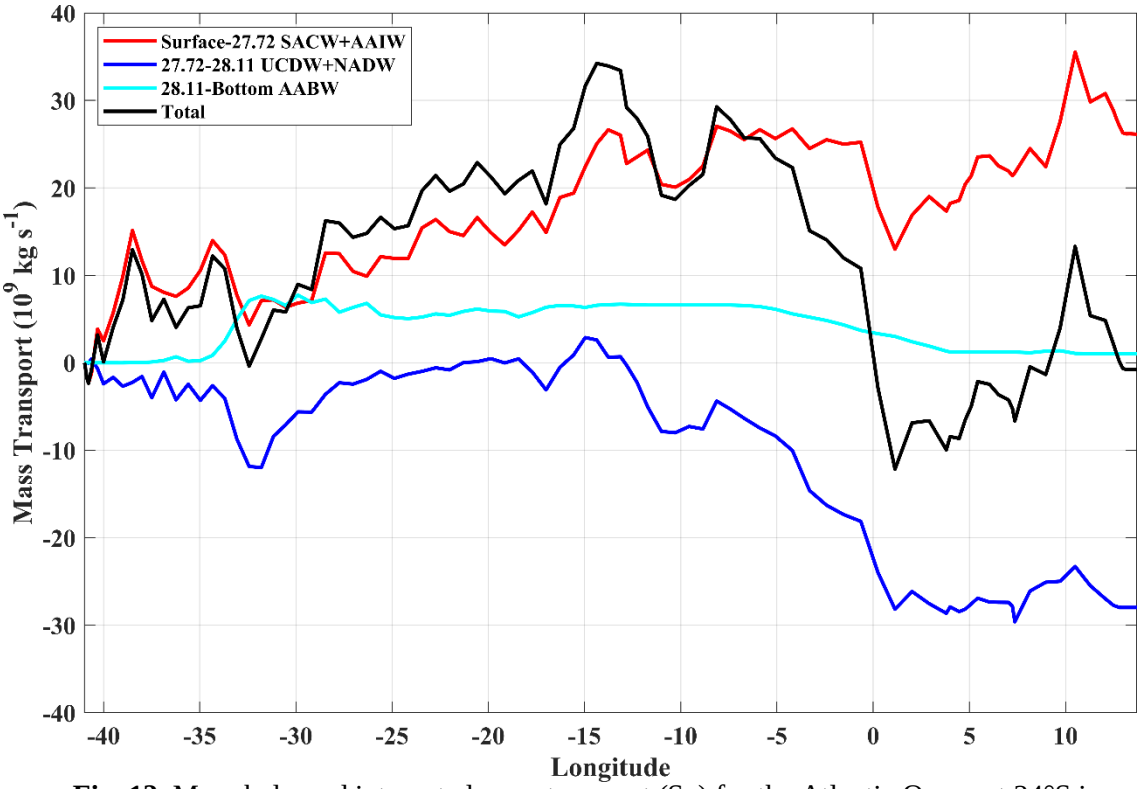

Fig. 12. Mass-balanced integrated mass transport (Sv) for the Atlantic Ocean at 24°S in 2009. The integration begins in the east at the coast of South America. Positive accumulated mass transport is northward. The legend shows the neutral surface layers γ^n (kg/m^3) where the waters masses spread.

4.1 Heat and Freshwater Transports

The estimated meridional heat flux across the A095 section is 1.0±0.1 PW, higher than the value that Bryden et al., (2011) obtained for the same time and region of study (0.7±0.1 PW). The agreement between the two positive values implies that the heat flux is significantly above zero, hence, the heat is being transported northwards in the south Atlantic Ocean.

In regards to the freshwater transport, our result confirms what Bryden et al., (2011) have displayed in their work: a net freshwater flux of -0.8±0.2 Sv for this section, which shows a significant loss of freshwater to the atmosphere (evaporation).

5. Conclusions and Discussion

The western and eastern boundary currents of the south Atlantic's subtropical gyre have been found in the region of study with estimated transports of -3.3±1.0 Sv and 13.2±3.3 Sv, respectively. These results are not significantly different from previous studies. In particular, Schmid & Majumder (2018) estimated the western and eastern transports to be -4.4±1.4 Sv and 9.6±2.8 Sv, respectively.

The NADW flow in these two regions matches also the previous studies: the DWBC transports these waters from the northern to the southern hemisphere of the Atlantic Ocean through the deep western boundary, and at lower latitudes of the southern hemisphere occurs its division into two branches, which can be seen in Figs. 5 and 12 (McDonagh & King, 2005). The transport of NADW by the DWBC has a net value (sum of the two branches) of -25.5±1.3 Sv (Fig. 12) somewhat higher than the McDonagh & King (2005) estimation (-20±2 Sv at 30ºS). Thus, the DWBC seems to decrease with higher latitudes in the South Atlantic, confirming what has been said in previous works (Bryden et al., 2011; Ganachaud, 1999; Garzoli et al., 2013).

The heat transport in the region is higher than the suggested in Bryden et al., (2011): 1.0±0.1 PW instead of 0.7±0.1 PW. Both are positive, which implies the heat transport is directed northward. A higher value of the heat transport in the South Atlantic Ocean might imply a higher net heat transport arriving to the North Pole, where this heat excess would be partially exchanged with the atmosphere and decreased in the atmosphere-ocean boundary layer by turbulent processes, or partially distributed in both the ocean and the atmosphere. Hence, the change in the overall ocean or atmosphere dynamics might not be significant with this small change in the heat transport.

The freshwater budget is also important for understanding the role of the South Atlantic Ocean in the global circulation scheme. In this region, the freshwater budget is -0.8±0.2 Sv (negative is loss of freshwater to the atmosphere), which is statistically the same value as the one estimated by McDonagh & King, (2005) at 45ºS (-0.7 Sv). Since the method of integrated surface climatology gives a value of 0.2±0.1 Sv, which would imply a gain of freshwater by the South Atlantic Ocean, a further study comparing the different methods and their possible results would be recommended (McDonagh & King, 2005).

In any case, it has been widely agreed that the North Atlantic Ocean is a very important zone of water mass subduction caused partially by the evaporative nature of the South Atlantic Ocean and the northward heat transport that takes places inside of it. Therefore, the results provided in this work agree with the theoretical base.

The present work can be improved by adding more constraints to the inverse model and studying the isoneutrals used in the region. Also, the addition of Acoustic Doppler Current Profiler (ADCP) measurements and the study of the anomalies of properties, such as temperature and salinity, could lead to several other results as well as enhancements of the already displayed ones.

Appendix

Table 1
List of Acronyms

Name	Acronym
Antarctic Bottom Water	AABW
Antarctic Intermediate Water	AAIW
Agulhas Current	AC
Atmospheric Model Intercomparison Project Reanalysis	AMIP-II
Brazil Current	BC
Benguela Current System	BCS
Circumpolar Deep Water	CDW
Conductivity-Temperature-Depth	CTD
Denmark Strait Overflow Water	DSOW
Deep Western Boundary Current	DWBC
Eastern Boundary Current	EBC
Global Ocean Ship-based Hydrographic Investigations Program	GO-SHIP
Iceland Scotland Overflow Water	ISOW
Labrador Sea Water	LSW
Malvinas Current	MC
Mediterranean Water	MW
North Atlantic Deep Water	NADW
South Atlantic Deep Water	SACW
Thermohaline Circulation	THC

Upper Circumpolar Deep Water	UCDW
Western Boundary Current	WBC
Walvis Ridge	WR

6. References

Backus, G. E., & Gilbert, J. F. (1967). Numerical Applications of a Formalism for Geophysical Inverse Problems. *Geophysical Journal International*, *13*(1–3), 247–276. https://doi.org/10.1111/j.1365-246X.1967.tb02159.x

Bashmachnikov, I., Neves, F., Calheiros, T., & Carton, X. (2015). Properties and pathways of Mediterranean water eddies in the Atlantic. *Progress in Oceanography*, *137*, 149–172. https://doi.org/10.1016/J.POCEAN.2015.06.001

Bryden, H. L., King, B. A., & McCarthy, G. D. (2011). South Atlantic overturning circulation at 24°S. *Journal of Marine Research*, *69*(1), 38–55. https://doi.org/10.1357/002224011798147633

Casanova-Masjoan, M., Pelegrí, J. L., Sangrà, P., Martínez, A., Grisolía-Santos, D., Pérez-Hernández, M. D., & Hernández-Guerra, A. (2017). Characteristics and evolution of an Agulhas ring. *Journal of Geophysical Research: Oceans*, *122*(9), 7049–7065. https://doi.org/10.1002/2017JC012969

Coachman, L. K., & Aagaard, K. (1988). Transports through Bering Strait: Annual and interannual variability. *Journal of Geophysical Research*, *93*(C12), 15535. https://doi.org/10.1029/JC093iC12p15535

Ferreira, M. L. de C., & Kerr, R. (2017). Source water distribution and quantification of North Atlantic Deep Water and Antarctic Bottom Water in the Atlantic Ocean. *Progress in Oceanography*, *153*, 66–83. https://doi.org/10.1016/J.POCEAN.2017.04.003

Ganachaud, A. (1999). Large scale oceanic circulation and fluxes of freshwater, heat, nutrients and oxygen. In Massachusetts Institute of Technology, Cambridge, USA. https://doi.org/10.1575/1912/4130

Ganachaud, A. (2003). Error Budget of Inverse Box Models: The North Atlantic. *Journal of Atmospheric and Oceanic Technology*, *20*(11), 1641–1655. https://doi.org/10.1175/1520-0426(2003)020<1641:EBOIBM>2.0.CO;2

García-Ibáñez, M. I., Pardo, P. C., Carracedo, L. I., Mercier, H., Lherminier, P., Ríos, A. F., & Pérez, F. F. (2015). Structure, transports and transformations of the water masses in the Atlantic Subpolar Gyre. *Progress in Oceanography*, *135*, 18–36. https://doi.org/10.1016/J.POCEAN.2015.03.009

Garzoli, S. L., Baringer, M. O., Dong, S., Perez, R. C., & Yao, Q. (2013). South Atlantic meridional fluxes. *Deep Sea Research Part I: Oceanographic Research Papers*, *71*, 21–32. https://doi.org/10.1016/J.DSR.2012.09.003

Hernández-Guerra, A., & Talley, L. D. (2016). Meridional overturning transports at 30°S in the Indian and Pacific Oceans in 2002–2003 and 2009. *Progress in Oceanography*, *146*, 89–120. https://doi.org/10.1016/J.POCEAN.2016.06.005

Hogg, N. G., Siedler, G., Zenk, W. (1999). Circulation and Variability at the Southern Boundary of the Brazil Basin. *Journal of Physical Oceanography*, *29*(2), 145–157. https://doi.org/10.1175/1520-0485(1999)029<0145:CAVATS>2.0.CO;2

Kanamitsu, M., Ebisuzaki, W., Woollen, J., Yang, S.-K., Hnilo, J. J., Fiorino, M., & Potter, G. L. (2002). NCEP–DOE AMIP-II Reanalysis (R-2). *Bulletin of the American Meteorological Society*, *83*(11), 1631–1644. https://doi.org/10.1175/BAMS-83-11-1631

Larque, L., Maamaatuaiahutapu, K., & Garcon, V. (1979). Deep-sea research. Part B, Oceanographic literature review. In *Oceanographic Literature Review* (Vol. 1). Retrieved from https://www.infona.pl/resource/bwmeta1.element.elsevier-b7288468-09ae-3cba-8545-d867e1d01116

McDonagh, E. L., & King, B. A. (2005). Oceanic Fluxes in the South Atlantic. *Journal of Physical Oceanography*, *35*(1), 109–122. https://doi.org/10.1175/JPO-2666.1

Munk, W. H. (1950). On The Wind-driven Ocean Circulation. *Journal of Meteorology*, *7*(2), 80–93. https://doi.org/10.1175/1520-0469(1950)007<0080:OTWDOC>2.0.CO;2

Parker, R. L. (1977). Understanding Inverse Theory. *Annual Review of Earth and Planetary Sciences*, *5*(1), 35–64. https://doi.org/10.1146/annurev.ea.05.050177.000343

Reid, J. L. (1989). On the total geostrophic circulation of the South Atlantic Ocean: Flow patterns, tracers, and transports. *Progress in Oceanography*, *23*(3), 149–244. https://doi.org/10.1016/0079-6611(89)90001-3

Rhein, M., Fischer, J., Smethie, W. M., Smythe-Wright, D., Weiss, R. F., Mertens, C., Putzka, A. (2002). Labrador Sea Water: Pathways, CFC Inventory, and Formation Rates. *Journal of Physical Oceanography*, *32*(2), 648–665. https://doi.org/10.1175/1520-0485(2002)032<0648:LSWPCI>2.0.CO;2

Schmid, C., & Majumder, S. (2018). Transport variability of the Brazil Current from observations and a data assimilation model. *Ocean Science*, *14*(3), 417–436. https://doi.org/10.5194/os-14-417-2018

Sprintall, J., & Tomczak, M. (1993). On the formation of central water and thermocline ventilation in the southern hemisphere. *Deep Sea Research Part I: Oceanographic Research Papers*, *40*(4), 827–848. https://doi.org/10.1016/0967-0637(93)90074-D

Stommel, H. (1948). The westward intensification of wind-driven ocean currents. *Transactions, American Geophysical Union*, *29*(2), 202. https://doi.org/10.1029/TR029i002p00202

Stommel, H., Arons, A. B., & Faller, A. J. (1958). Some Examples of Stationary Planetary Flow Patterns in Bounded Basins. *Tellus*, *10*(2), 179–187. https://doi.org/10.3402/tellusa.v10i2.9238

Suga, T., & Talley, L. D. (1995). Antarctic Intermediate Water circulation in the tropical and subtropical South Atlantic. *Journal of Geophysical Research*, *100*(C7), 13441. https://doi.org/10.1029/95JC00858

Sverdrup, H. U. (1947). Wind-Driven Currents in a Baroclinic Ocean; with Application to the Equatorial Currents of the Eastern Pacific. *Proceedings of the National Academy of Sciences of the United States of America*, *33*(11), 318–326. https://doi.org/10.1073/pnas.33.11.318

Talley, L.D., Feely, R. A., Sloyan, B. M., Wanninkhof, R., Baringer, M. O., Bullister, J. L., Zhang, J.-Z. (2016). Changes in Ocean Heat, Carbon Content, and Ventilation: A Review of the First Decade of GO-SHIP Global Repeat Hydrography. *Annual Review of Marine Science*, *8*(1), 185–215. https://doi.org/10.1146/annurev-marine-052915-100829

Talley, Lynne D. (2003). Shallow, Intermediate, and Deep Overturning Components of the Global Heat Budget. *Journal of Physical Oceanography*, *33*(3), 530–560. https://doi.org/10.1175/1520-0485(2003)033<0530:SIADOC>2.0.CO;2

Talley, Lynne D., Pickard, G. L., Emery, W. J., & Swift, J. H. (2011). *Descriptive physical oceanography : an introduction* (Sixth Edit; Elsevier, ed.). Academic Press.

Tsuchiya, M., Talley, L. D., & McCartney, M. S. (1994). Water-mass distributions in the western South Atlantic; A section from South Georgia Island (54S) northward across the equator. *Journal of Marine Research*, *52*(1), 55–81. https://doi.org/10.1357/0022240943076759

Warren, B. A., & Speer, K. G. (1991). Deep circulation in the eastern South Atlantic Ocean. *Deep Sea Research Part A. Oceanographic Research Papers*, *38*, S281–S322. https://doi.org/10.1016/s0198-0149(12)80014-8

Wunsch, C. (1996). The Ocean Circulation Inverse Problem. In *The Ocean Circulation Inverse Problem*. https://doi.org/10.1017/cbo9780511629570.006

Zenk, W., & Armi, L. (1990). The complex spreading pattern of Mediterranean Water off the Portuguese continental slope. *Deep Sea Research Part A. Oceanographic Research Papers*, *37*(12), 1805–1823. https://doi.org/10.1016/0198-0149(90)90079-B